Not to appear in Nonlearned J., 45.
Preprint typeset using LaTeX style emulateapj v. 01/23/15

THE RELATIONSHIP BETWEEN SIZE AND STAR FORMATION IN ACTIVE GALAXIES

J. I. Phillips[1], Kareem El-Badry, Hugh Dickinson[1], Claudia Scarlata [1], Evan Skillman[1], others(?)
Minnesota Institute for Astrophysics, University of Minnesota, Minneapolis, MN 55455
Not to appear in Nonlearned J., 45.

ABSTRACT

We examine a sample of SDSS galaxies with stellar masses between $10^{8.5}$ and 10^{11} $M_\odot$ for signatures of radial feedback driven by bursty star formation. We measure each galaxy's offset from the median size-mass relation, and plot this size against their $H\alpha$ emission. Below $10^{9.5}$ $M_\odot$, we see a positive correlation between galaxy concentration and $H\alpha$ emission, i.e., actively star-forming galaxies are more concentrated. This is observational evidence for a "breathing" mode of star formation, where intense star formation in the galactic center drives radial outflows of gas and stars in a cyclic fashion. More massive galaxies do not show the same correlations between size and star formation activity, consistent with the observations that these objects reside in cuspy dark matter halos.

1. INTRODUCTION

Dwarf galaxies, galaxies at or below stellar mass of $\sim 10^9 M_\odot$, are important laboratories that allow us to study structure formation at the smallest scales. In particular, their ratios of baryons to dark matter are extremely low, typically around 1:100. This gives rise to important differences in the structure and star formation histories of dwarf galaxies as compared to more massive galaxies ($M_\star > 10^9 M_\odot$), and studying these differences can shed light on important physics related to how galaxy formation is regulated by both baryons and dark matter.

Cosmological simulations based on the preferred cold dark matter model (ΛCDM) predict that galaxies form in self-similar halos of dark matter, which have density profiles described by a double power law with an inner logarithmic slope of -1, termed a Navarro-Frank-White (NFW) profile (Navarro et al. 1997). The distribution statistics and kinematics of massive galaxies is fully consistent with them living in dark matter halos with NFW profiles (Wambsganss et al. 2004; Springel et al. 2005; Boylan-Kolchin et al. 2009; Klypin et al. 2011); however, dwarf galaxy kinematics are better described by halos with a flat inner slope, typically referred to as a "cored" profile (Moore 1994; McGaugh et al. 2001; Marchesini et al. 2002; Simon et al. 2005; de Blok et al. 2008). This tension between predictions made from ΛCDM and observations is termed the "core-cusp problem." A closely related problem, the "too big to fail problem," notes that satellite halos (or subhalos) seen around Milky-Way-like galaxies in ΛCDM simulations are too dense to host any of the observed Milky Way dwarf satellites (Boylan-Kolchin et al. 2011, 2012). Note that these two problems may indeed be two manifestations of the same problem, i.e., both problems may be solved if halos in the real Universe have cored profiles. Recent work by Garrison-Kimmel et al. (2014) demonstrated that the "too big to fail" problem extended beyond the Milky Way's virial radius, suggesting that the problem has more to do with how dwarf galaxies form than how environmental effects such as ram-pressure stripping or tidal interactions manifest (See, e.g., Gunn & Gott (1972); Larson et al. (1980); Farouki & Shapiro (1981); Moore et al. (1996); Balogh et al. (2000) for a discussion of these effects).

In order to resolve these problems, one of two things must be true. Either the underlying physics of ΛCDM must be modified in some way, or baryonic processes must be invoked to bridge the gap between theory and observation. Recent work has been dedicated to exploring both possibilities. On the cosmological side, both self-interacting dark matter and warm dark matter can serve to suppress structure formation and lower the central densities of dark matter halos (Lovell et al. 2014; Elbert et al. 2015). With respect to baryonic matter, supernova feedback has long been known to deposit energy into the interstellar medium (ISM), driving galactic winds (Larson 1974; Dekel & Silk 1986). More recently, this feedback has been posited as a mechanism by which energy may be injected into dark matter particles, kinematically warming them. Several authors have argued that if star formation proceeds in bursts in dwarf galaxies, energy will be injected with enough efficiency to create cores in the centers of dark matter halos (Governato et al. 2010, 2012; Pontzen & Governato 2012a). Observational studies have demonstrated that, for dwarf galaxies in particular, the star formation rate as measured by $H\alpha$ has more scatter than the star formation rate as measured by FUV emission (Sullivan et al. 2000; Boselli et al. 2009; Lee et al. 2009; Shivaei et al. 2015; Guo et al. 2016; Sparre et al. 2017). Since these indicators trace star formation over different timescales, these studies are consistent with a picture where star formation in dwarfs is stochastically bursty; however, radial transport driven by this stochastic star formation remains unobserved.

One clue to resolving this dilemma may lie in how dwarf galaxies' old stars are distributed. While exceptions abound, massive galaxies generally have concentrations of old stars in the center, and younger stars in the outskirts (de Jong 1996; Bakos et al. 2008). Dwarf galaxies, on the other hand, typically show the inverse; young stars in the center and old stars on the outskirts (Hidalgo et al. 2009, 2013). Several studies have argued that these radial age gradients arise from in situ formation; old stars in the external region were born there at early times and generally remained there, exhibiting only minor radial movement with no preferred direction (Stinson et al. 2009; Schroyen et al. 2013). However, recent simulations have raised the possibility that stars

in dwarf galaxies experience significant radial transport; young stars are born in galactic interiors, then at some point in their lifetimes they move to larger radii, possibly driven by feedback (González-Samaniego et al. 2016; El-Badry et al. 2016). Distinguishing between these two possibilities could shed light on the physics behind dwarf galaxy formation.

A unified model of galaxy formation that solves these problems was first put forward by Navarro et al. (1996), where the authors show that feedback driven outflows can produce galaxies in simulations with realistically cored profiles. Further studies (Governato et al. 2010, 2012; Maxwell et al. 2012; Di Cintio et al. 2014; Pontzen & Governato 2014; Chan et al. 2015; El-Badry et al. 2016) refined the theory, specifying that feedback regulates dwarf galaxy star formation in a stochastic manner and powers radial transport, but an observational smoking gun for this model remains elusive.

In this study, we use observations of both dwarf galaxies and massive galaxies to investigate the observational predictions of a model for dwarf galaxy formation whereby stochastic star formation in the center of the galaxy powers radial transport of both baryonic and dark matter. Specifically, our study will focus on the structure of star forming galaxies, and how that structure is dependent on the vigor with which the galaxy is forming stars. The paper is organized as follows: in Section 2, we discuss the data used in the study, in Section 3 we present our results, and in Section 4 we discuss the implications of the work. Throughout the paper we use h=0.7, and unless otherwise noted, star formation rates are calculated according to Kennicutt (1998).

2. DATA AND OBSERVATIONS

The data used in this study come from the Sloan Digital Sky Survey (SDSS, York et al. 2000), making use of the NYU and MPA-JHU value-added galactic catalogs (Kauffmann et al. 2003; Brinchmann et al. 2004; Blanton et al. 2005). To select our scientific sample, we first take all galaxies with stellar masses between 10^8 $M_\odot$ and 10^{11} $M_\odot$. We require galaxies in our scientific sample to be actively star forming, so we impose a minimum $H\alpha$ equivalent width of 2Å and require that the galaxies we select reside in the star forming region of the BPT diagram (Baldwin et al. 1981). We admit to the scientific sample only galaxies within a mass-dependent completeness redshift, estimated by dividing the sample into five mass bins of width 0.5 dex and plotting a histogram of the redshift of galaxies in each bin. The peak of the histogram was taken to be the approximate completeness limit for the scientific sample. These limits, as well as the number of galaxies in our sample, are given in Table 1. In Figure 1 we plot the star formation rate of the galaxies in our sample versus their physical size. We note that galaxies above masses of $10^{9.5}$, we see few low star formation rate objects with large size, as seen by Patel et al. (2018), but this trend goes away at lower masses.

2.1. *Central star formation*

SDSS spectroscopy is based on light being channeled into fibers 3 arcsec in diameter. This gives us an opportunity to more closely probe the star formation rate in the galaxy's central regions. Since we will be interested in star formation happening in the galaxy's center, we will define a fiber-corrected star formation rate that intentionally over weights the fiber measurement taken at the galaxy center, which we will call $SFR_{\rm cent}$. Eventually, we will be interested in whether or not $SFR_{\rm cent}$ is larger or smaller than the galaxy's true star formation rate, which will give us a measure of how centrally concentrated the star formation is, but first we will detail how $SFR_{\rm cent}$ is calculated.

We begin by defining a parameter Ψ that corresponds to the fraction of a galaxy's area on the sky that lies within the fiber. For galaxies smaller than 3 arcsec, $\Psi = 1$. For larger galaxies, $\Psi = \frac{A_z}{\pi R^2}$, where R is the circularized radius of the galaxy measured in kpc (taken to be r-band R90 so as to account for nearly all light from the galaxy) and A_z is the area of a circle of diameter 3 arcsec at the redshift of the galaxy. Figure 2 shows Ψ plotted against galaxy radius for galaxies in our $10^{9.5} - 10^{10}$ $M_\odot$ bin. Notice that, as one might expect, larger galaxies tend to have more of their area fall outside out the fiber, leading to lower values of Ψ. The selection effect in the upper right portion of the plot is introduced by the redshift cut we place on the sample. An object that lies on this line is located close to the maximum allowed redshift, such that it is the minimum size on the sky, and thus the largest Ψ.

If we are carrying out a correction on some generic parameter Θ, which could represent e.g. star formation rate, we assume that the correction will take the form of a power law, i.e.,

$$\Theta_{\rm total} = \Theta_{\rm fiber} \times \Psi^{-\alpha}.$$

Here α is a power law index that we will derive empirically and $\Theta_{\rm fiber}$ is the measured value of Θ within the fiber. In calculating α, our goal is to correct Θ such that its distribution is independent of redshift. We assume no redshift evolution within our full sample, which is a fair assumption between z=0 and z=0.07. Then we fit a linear relationship to $\log \Theta_{fiber}$ and $\log \Psi$. The slope of this relationship we adopt as α. This fitting procedure can be seen in Figure 3.

To validate that our correction procedure does indeed produce a measure for Θ that is independent of redshift, we divide each mass bin into a low redshift subsample and high redshift subsample[1]. Galaxies with redshift less than $z_{complete}/2$ are placed in the low redshift subsample, and with redshifts between $z_{complete}/2$ and $z_{complete}$ in the high redshift sample. In applying the correction, we will call the measured value of the parameter of interest Θ_{fiber}. We then compare the distributions in Θ_{total} between the low and high redshift sample. This comparison is shown in H_α luminosity in Figure 4 for the $M_\star \sim 10^{9.5} M_\odot$ bin. We see excellent agreement in the corrected values across redshift for each mass bin, and note that this agreement is only seen after the correction is made. Table 1 contains the measured alphas for each sample mass bin. If we substitute SFR for the generic Θ in the above derivation, we can make explicit the definition

$$SFR_{\rm cent} \equiv SFR_{\rm fiber} \times \Psi^{-\alpha}$$

[1] We use "high" redshift in a relative sense; all galaxies we consider in this paper are quite low redshift.

Mass Bin ($M_\odot$)	α	$z_{\rm complete}$	N
$10^{8.5} - 10^{9.0}$	0.797	0.023	13732
$10^{9.0} - 10^{9.5}$	0.830	0.035	29979
$10^{9.5} - 10^{10.0}$	0.895	0.058	58709
$10^{10.0} - 10^{10.5}$	0.698	0.081	88476
$10^{10.5} - 10^{11.0}$	0.731	0.15	69858

Table 1
Power law index, completeness redshift, and number count of galaxies in each mass bin we consider.

.

2.2. *Concentration/luminosity degeneracy*

As previously mentioned, the above procedure produces a measure for $SFR_{\rm cent}$ that is overly reliant on information from the galaxy's center. If two galaxies have the same Ψ and $SFR_{\rm fiber}$, they would end up with the same $SFR_{\rm cent}$, even if one of them had substantially more star formation in its outskirts (and thus a higher true star formation rate). Essentially, using the parameter $SFR_{\rm cent}$ introduces a degeneracy between a galaxy's true star formation rate and the concentration of its star formation. Note that, had we simply corrected for the area outside of the fiber (i.e., applied an $\alpha = 1$ correction), we would have been degenerate in redshift as well.

To investigate this degeneracy, we carried out a simple Monte Carlo simulation with toy models of galaxies. The galaxies were divided into an inner and outer region, each with a separate star formation density. Galaxies were divided into two categories: those with greater star formation rate density in the center, and those with greater star formation rate density in the outskirts; i.e. galaxies with central star formation and galaxies with star formation in the disk. We then applied the same steps described above to determine a $SFR_{\rm cent}$ for our simulated galaxies. To remove the variation due to intrinsic star formation, we normalize $SFR_{\rm cent}$ by each galaxy's intrinsic star formation rate. This allows us to examine $\log \frac{SFR_{\rm cent}}{SFR}$ for each galaxy as the "central excess" in star formation. Upon plotting $\frac{SFR_{\rm cent}}{SFR}$ vs. Ψ, for the toy galaxies, the two models occupy distinct regions of parameter space, with the objects centrally concentrated star formation having the highest $\frac{SFR_{\rm cent}}{SFR}$ and those with low central star formation displaying the lowest $\frac{SFR_{\rm cent}}{SFR}$. This is shown in the left panel of Figure 5. If we color the points in $\log \frac{SFR_{\rm cent}}{SFR}$ vs. Ψ space by concentration (i.e., R90/R50) we can see a correspondence between high $\log \frac{SFR_{\rm cent}}{SFR}$ and concentration, as shown in the right panel of Figure 5. We will therefore use the ratio between $SFR_{\rm cent}$ and SFR as a proxy for the concentration of star formation in our galaxies. Note that while $\log \frac{SFR_{\rm cent}}{SFR}$ can serve as a proxy for concentration, we can not establish a one-to-one mapping between $\log \frac{SFR_{\rm cent}}{SFR}$ and concentration.

3. RESULTS

In this section we will examine the relationship between a galaxy's physical size (as probed by r-band R90) and the rate and concentration of its star formation. By dividing our sample into bins of 0.5 dex in stellar mass, we can examine how the relationship between size and $H\alpha$ emission varies with galaxy mass. Of particular interest is what happens at dwarf-scale masses, i.e., the lowest two mass bins of our sample.

To establish a mass-independent size metric, we fit a mass-size relation to all star-forming galaxies below redshift 0.03, then determine the expected size for each galaxy in the sample based on its stellar mass. For each galaxy, we then calculate a "size offset" which is the logarithm of the ratio between the actual size of the galaxy in kpc and the expected size of that galaxy, also in kpc. This size offset parameter has the useful properties of being centered at or very close to zero for any given population of galaxies, and having relatively consistent scatter (about 0.4 dex) over the mass ranges we probe.

In Figure 6, we plot star formation rate against size offset for galaxies in each mass bin. As expected, star formation tends to increase with increasing mass. Within each mass bin, we plot the average star formation rate at fixed size offset as a blue line. The broad trend we see is a positive slope from in the dwarf-scale mass bins, such that smaller galaxies are relatively less star forming, which transitions to a nearly flat relation in the highest mass bin.

If, however, we plot the slope of our size/star formation rate relation against the stellar mass of the galaxies in each bin (Figure 7), we see a more complicated behavior. Rather than monotonically decreasing with stellar mass, the slope turns over $10^{8.5} M_\odot$ and again at $10^{9.5} M_\odot$. The size of the error bars makes it unclear whether or not the turnover at $10^{8.5} M_\odot$ is real, however the turnover at $10^{9.5} M_\odot$ seems to indeed be real.

We see a very similar result when we examine the star formation rate density[2] with respect to size and mass. Figure 8 shows the average star formation rate density plotted against size offset for galaxies in our six bins, while Figure 9 shows the dependence of the slope of that relation on galactic stellar mass. Unsurprisingly, we see essentially the same trends, with a strong maximum at $10^{9.5} M_\odot$ and a weak minimum at $10^{8.5} M_\odot$.

3.1. *Central Star Formation*

In section 2.2, we discuss how the ratio $log \frac{SFR_{\rm cent}}{SFR}$, which describes the deviation in total star formation implied by the galaxy's center from the true star formation rate, can be used to probe galaxy concentration. We turn now to examining how this ratio varies with galaxy size and mass.

In Figure 10, we plot the relationship between $log \frac{SFR_{\rm cent}}{SFR}$ and size offset for galaxies in the five mass bins. The first thing we notice is that large-sized objects in the 10^8 $M_\odot$ bin have highly enhanced $log \frac{SFR_{\rm cent}}{SFR}$ as compared to the rest of the sample, suggesting that these galaxies have significantly denser star formation than more massive objects. Among the other five bins, we a negative correlation in the $10^9 M_\odot$ bin gradually flatten with increasing mass. This is very apparent when we plot the slopes of these relations against stellar mass in Figure 11, and represents an enhancement in star formation density among small-size objects unique to dwarf galaxies.

Similarly, in Figure 10, we plot the relationship between $log \frac{SFR_{\rm cent}}{SFR}$ and star formation rate. First considering dwarf galaxies, we see no correlation in the 10^8 $M_\odot$ bin and a significant positive correlation in the $10^{8.5}$ $M_\odot$

[2] Where $\Sigma_{SFR} = SFR/\pi R_{90}^2$.

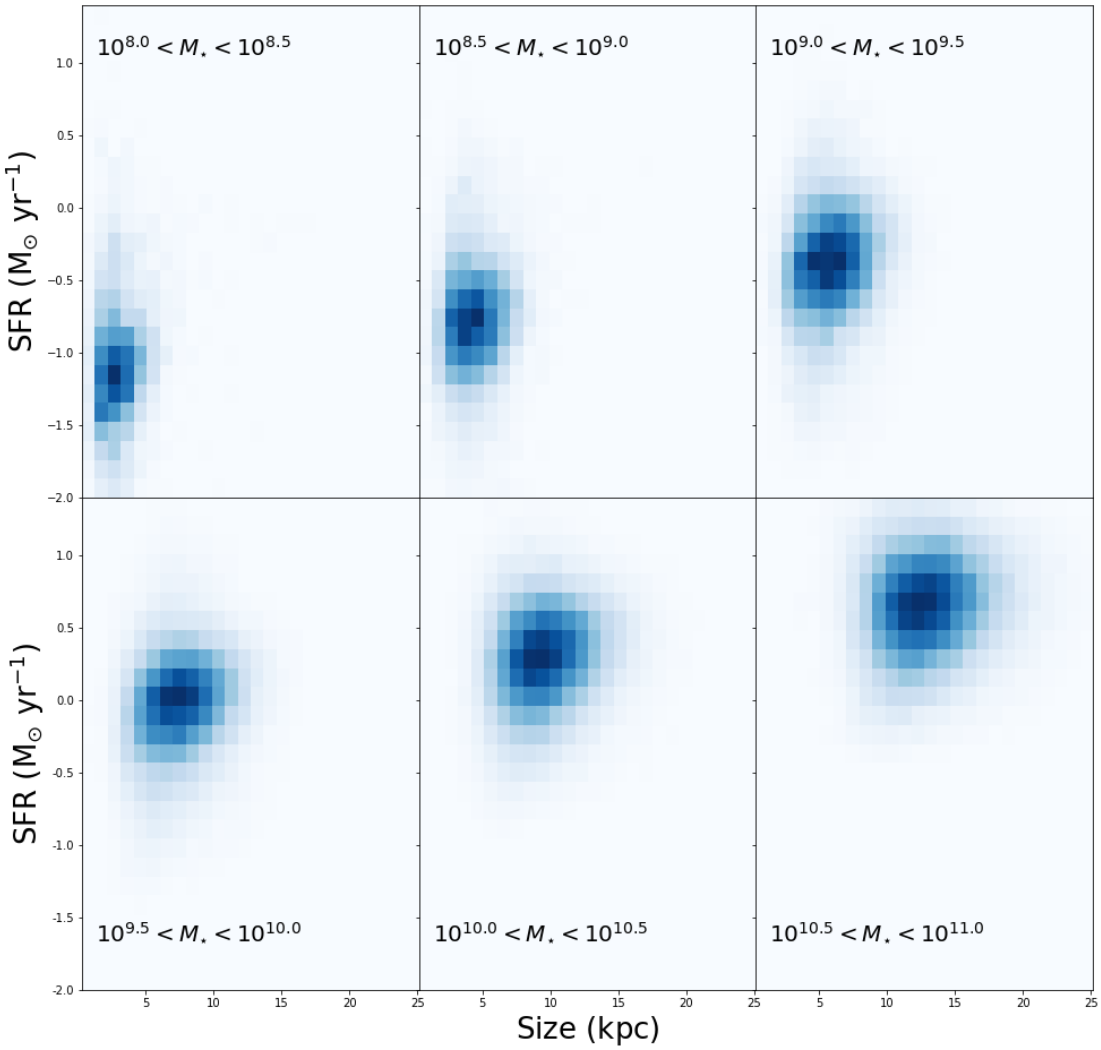

Figure 1. Histograms of star formation rate versus size for galaxies in our five mass bins. At high masses, we see a relative lack of objects with large sizes and low star formation rates, which goes away at small masses.

bin. We see a negative correlation in all other bins. The implication is that dwarfs with high star formation have concentrated star formation, while the opposite is true for more massive galaxies.

In Figure 14, we plot $\frac{SFR_{\rm cent}}{SFR}$ versus size offset for the $10^{8.5} M_\odot$ mass bin. We define with objects with $\frac{SFR_{\rm cent}}{SFR} > 0$ as centrally star forming objects, while galaxies with $\frac{SFR_{\rm cent}}{SFR} < 0$ are objects that preferentially form objects in the outer regions. These results are shown in the figure; the line through the two dimensional histogram separates these two populations. We measure the fraction of objects observed to be in the central phase to be 0.62, which under the assumption that these represent distinct phases in galactic evolution, is equivalent to a measurement of the duty cycle. In Section 4, we will use this value to comment on the physics at play in these systems.

4. DISCUSSION

4.1. *Galaxy Size*

An important prediction of the "breathing" model of feedback regulation in dwarf galaxies is that star formation rate is anti-correlated with galaxy size. In the model, stars are formed in the galactic center. Supernova feedback from these young stars then blows out the reservoir of gas from which the stars were formed, dampening star formation. As a result, galaxies are actively forming stars when they are at their smallest. During the subsequent blowout phase the galaxy will be more

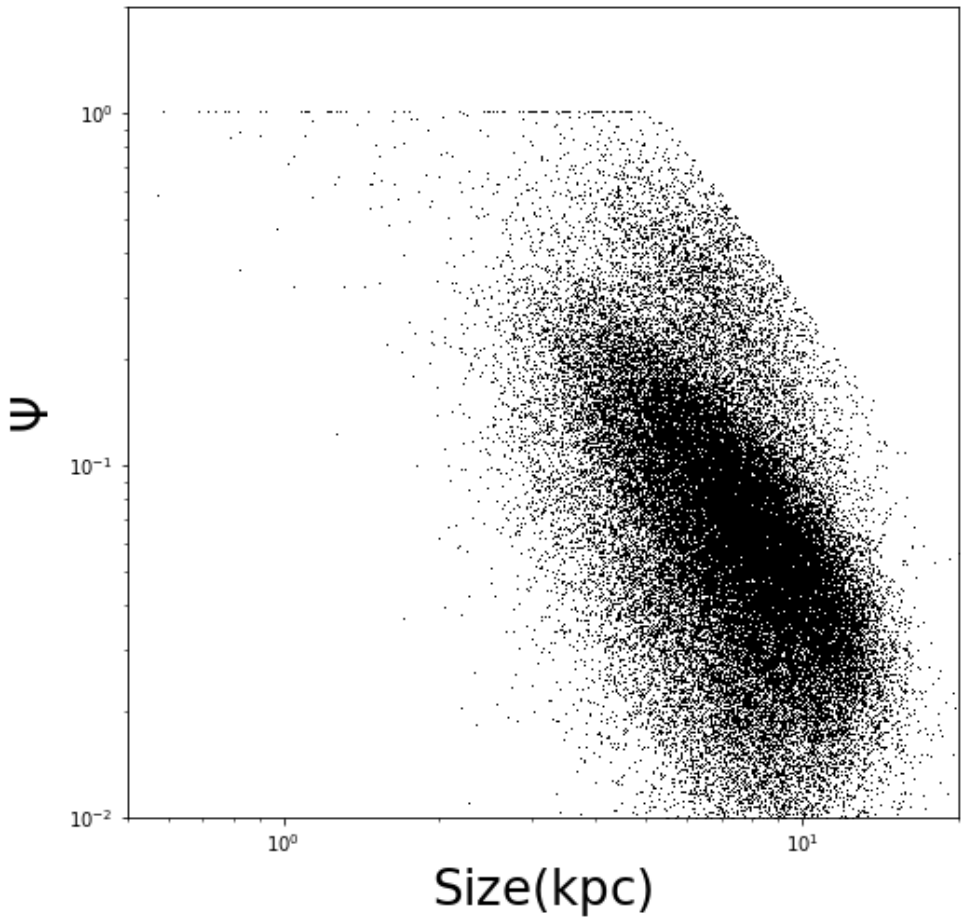

Figure 2. Geometric parameter Ψ plotted vs. physical size for galaxies in the $10^{9.5} - 10^{10} M_\odot$ mass bin. Ψ measures the fraction of the galaxy that falls within the SDSS fiber. The selection effect in the upper right corner arises due to the cut in redshift space.

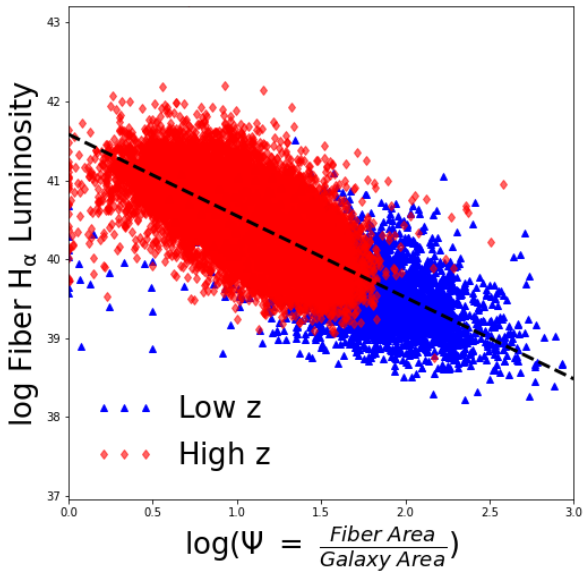

Figure 3. The relationship between the geometric factor Ψ measuring the ratio of a galaxy's size to the size of the SDSS fiber and the fiber H_α luminosity for galaxies in the $10^{9.5} - 10^{10} M_\odot$ bin. Knowing the average functional form of this relationship allows us to correct for fiber effects. Points marked with a blue triangle are at lower redshift than those marked with a red diamond

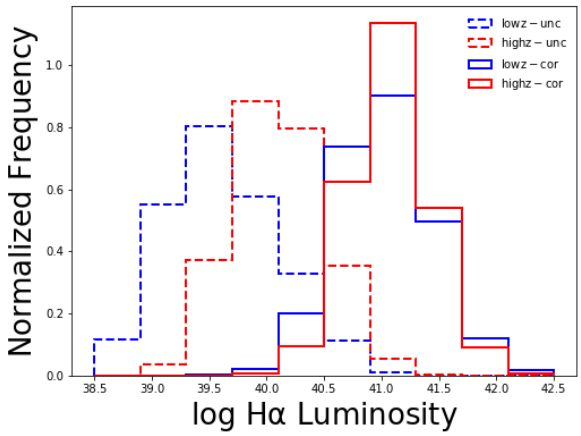

Figure 4. Histogram of $H\alpha$ luminosities for the uncorrected (dashed blue line) and corrected (solid blue line) low z calibration set, along with the uncorrected (dashed red line) and corrected (solid red line) high z calibration set. Correcting both sets brings them into agreement.

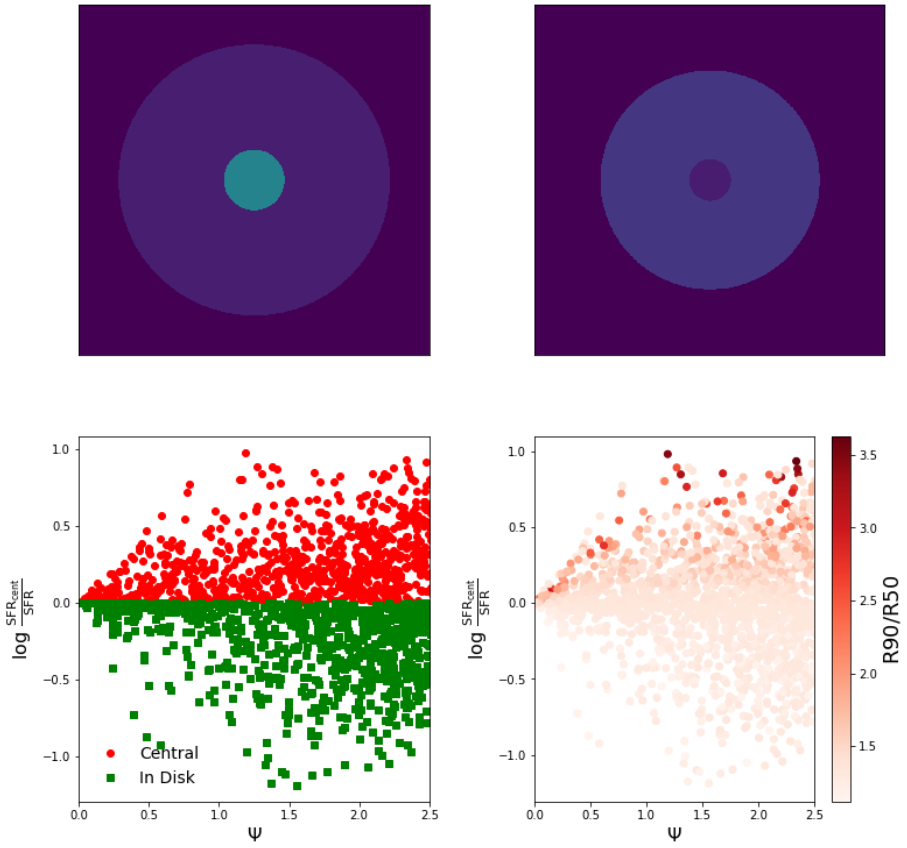

Figure 5. *Top:* Examples of allowed toy star-forming models; *left*: centrally concentrated star formation, *center*: constant star formation density, *right*: star formation preferentially in the outskirts. *Bottom:* log $SFR_{\rm cent}$ vs. Ψ colored by (*left*) model, and (*right*) concentration.

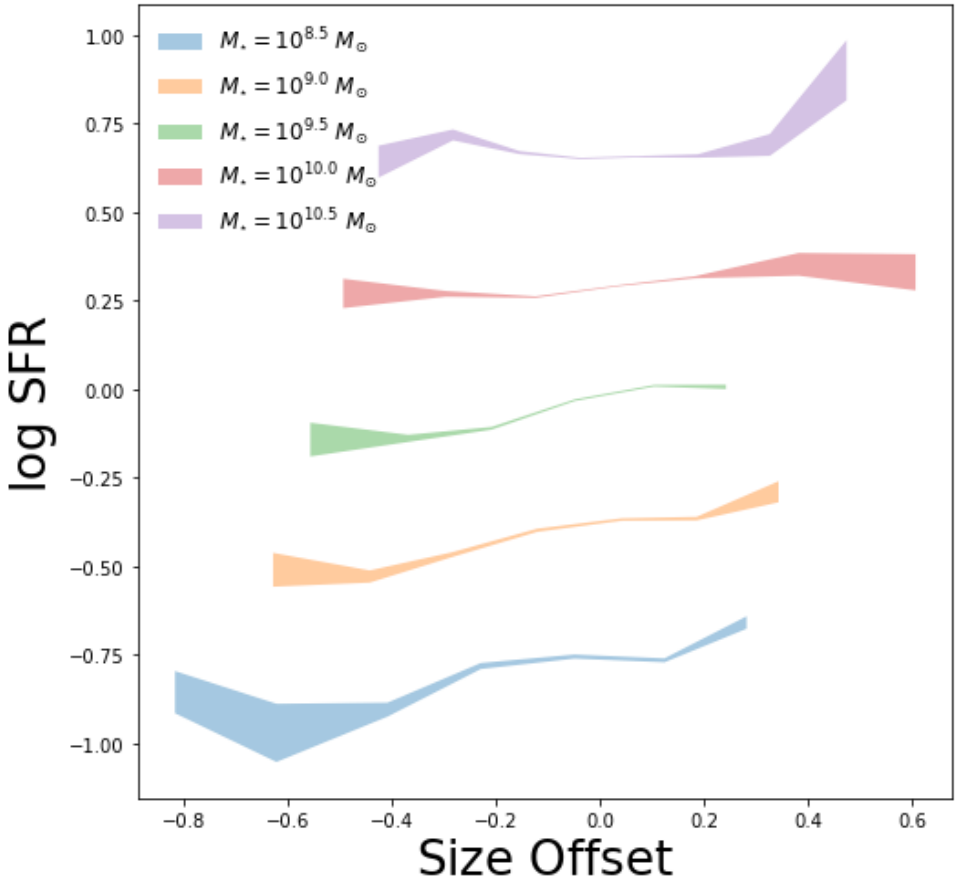

Figure 6. Star formation rate plotted against size offset for galaxies in five mass bins. Errors shown are the standard deviation of star formation rates for galaxies binned on size. Errors are computed similarly in subsequent similar plots.

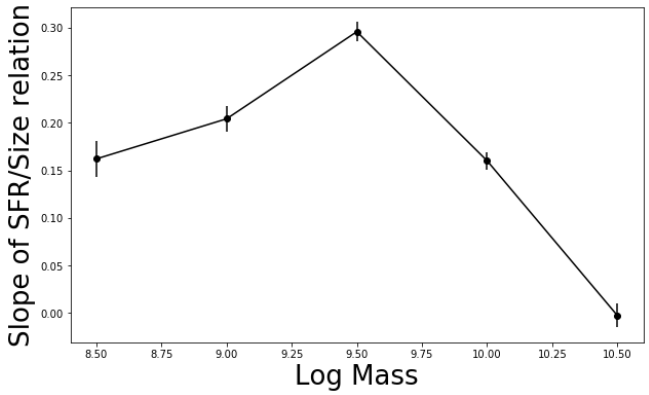

Figure 7. Slope of the star formation rate vs. size relation plotted against stellar mass. The slope is maximally steep in intermediate masses, and flattens at the low and high end. Errors shown are the standard error on the mean. Errors are computed similarly in subsequent similar plots.

diffuse and, if the galactic wind drives radial transport, the galaxy will have a larger effective radius (El-Badry et al. 2016).

We don't see an anti-correlation between size and star formation rate, meaning that this prediction of breathing is not borne out. However, we do see a relatively higher star formation rate among small-sized objects in dwarf mass ranges, as indicated by the decline in the slope of the star formation rate vs. size relation at small masses. This is consistent with a picture whereby small dwarf galaxies have somewhat enhanced star formation relative to their physical size over their intermediate-mass counterparts.

Furthermore, taking $\frac{SFR_{cent}}{SFR}$ as a proxy for concentration, we see an enhancement in concentration in small-size dwarf galaxies, seen as an inflection or "kink" in the concentration-size relationship as seen in Figure **??**. At higher masses, however, this relationship flattens, and the inflexion goes away. This trend could evidence for a breathing mode of feedback-regulated star formation in high-mass dwarfs. Indeed, the evidence from concentration is stronger than the evidence from size, suggesting that further investigation into where star formation occurs in dwarf galaxies is necessary.

There are, however, potential alternate explanations for the observed effects we point out. We will briefly discuss these. Firstly, we will consider the possibility that galaxies at different sizes do form stars at the same rate, but different amounts of $H\alpha$ emission could be produced per unit star formation. This could be due to variations in the initial mass function (IMF), which sets the rates at which stars of different masses form. A top-heavy IMF, where more massive stars are formed relatively more frequently, would result in more ionizing radiation being formed per unit star formation. Our results could potentially be explained by smaller galaxies having more top-heavy IMFs, and correspondingly relatively more H_α emission. Whether or not the IMF varies between galaxies, or within galaxies, is an area of active research, with

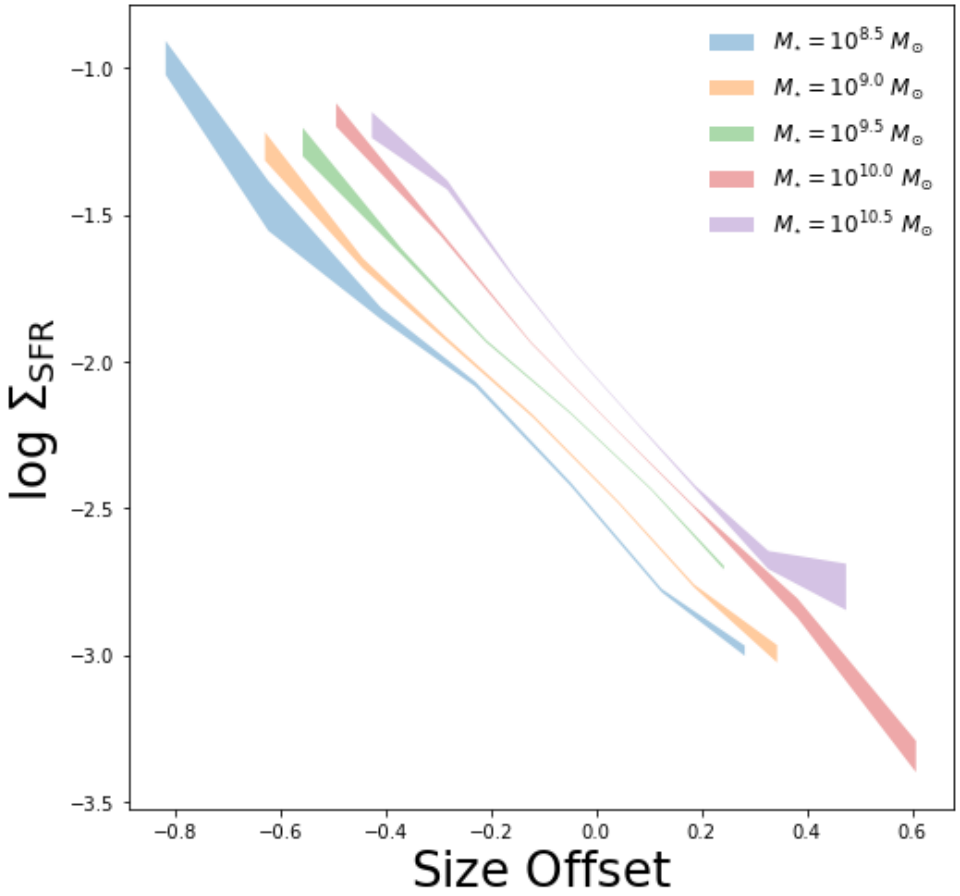

Figure 8. Star formation density rate plotted against size offset for galaxies in five mass bins. A negative correlation is seen in all five bins, with average star formation rate density increasing with mass.

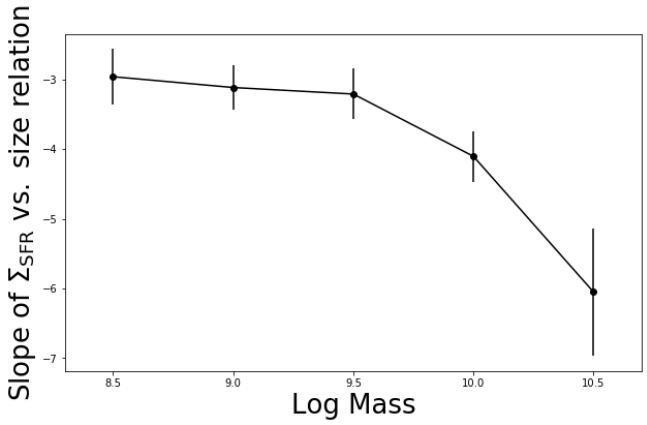

Figure 9. Slope of the star formation rate density vs. size relation plotted against stellar mass. Slopes were derived using orthogonal distance regression, and show a clear trend of steepening with increasing mass.

most results being consistent with a universal IMF (e.g., Lee et al. 2009; Bastian et al. 2010).

An alternate possibility is that galaxies form stars at the same rate and as described by the same IMF at the same mass, but dust obscures star formation in such a way as to create a trend where there would otherwise be none. However, previous studies have shown that dust reddening increases with increasing stellar mass (Garn & Best 2010), leaving it unlikely to drive an effect seen primarily at dwarf masses. We see a similar result in our data, with Balmer decrement increasing with increasing galaxy mass. Thus we conclude that dust extinction is unlikely to be the driver of the effects we see.

4.2. *Duty Cycle and Energetics*

In Section 3, we divide the galaxies in our lowest mass bin into objects forming stars in their centers (i.e. objects with high H_α concentrations) and objects forming stars in their outer regions (i.e. objects with low H_α concentrations) by drawing a line at $\frac{SFR_cent}{SFR} = 0$. Galaxies above that line are centrally star forming, while those below the line belong to the group forming stars in their outskirts. Assuming that these represent phases of star formation, we define the duty cycle of this population to be the fraction of time a galaxy spends in its central phase, as estimated by the fraction of galaxies observed to be in the central phase, and measure this value to be 0.60; i.e., dwarf galaxies spend roughly sixty percent of their lifespan in a phase where they most are actively forming stars in their centers and the other sixty percent not in this phase. Due to the increased size of the galaxy during the passively star forming phase, we will interpret this to be the phase where the galaxy is undergoing stellar feedback-driven blowouts. There are several different interpretations for this measured duty cycle that we now discuss.

Firstly, we will examine this number under the view

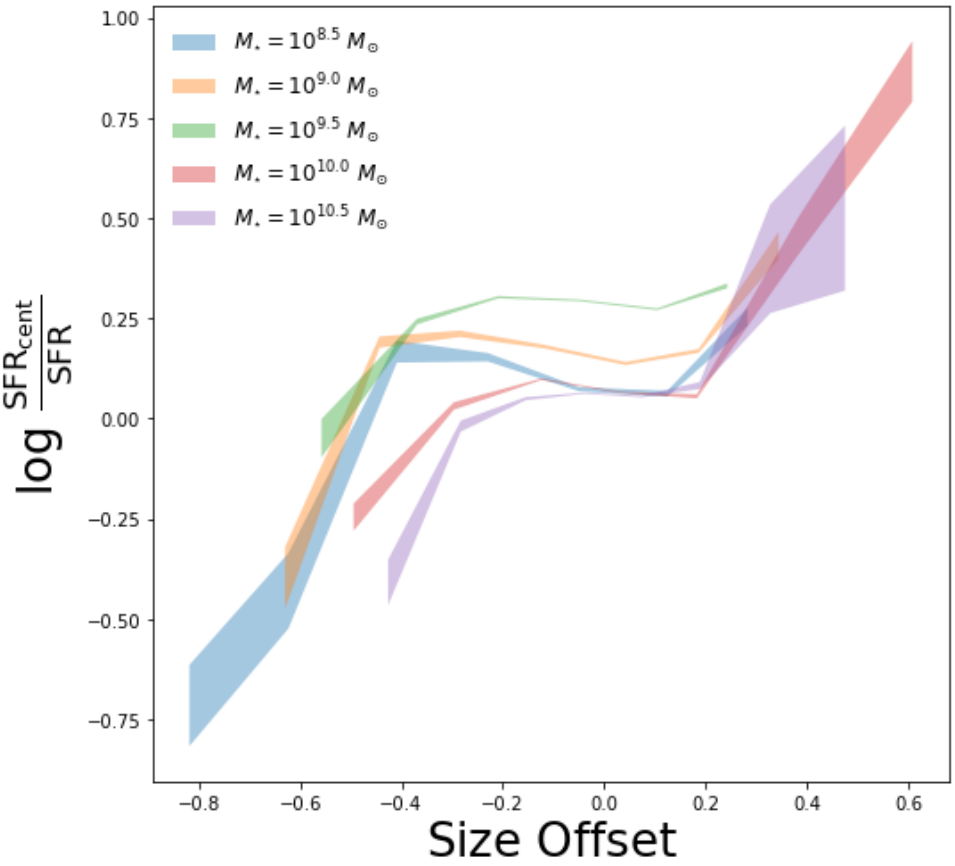

Figure 10. Star formation rate plotted against size offset for galaxies in five mass bins. The data transition from a nearly flat relation at small masses to a slight correlation at larger masses. Black and green points represent smaller-than-average and larger-than-average galaxies, respectively. Blue dashed line is a linear fit to the data.

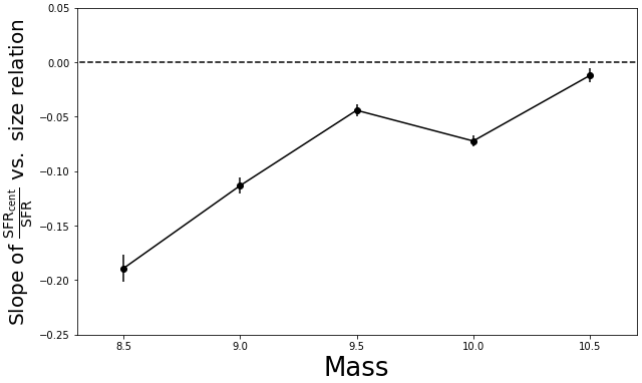

Figure 11. Slope of the $\frac{SFR_{cent}}{SFR}$ ratio vs. size relation plotted against stellar mass. The data point at $10^8 M_\odot$ is omitted because it lies well away from the other data points. The other five points show a clear negative correlation with stellar mass. At lower masses, smaller objects experience enhanced concentration.

that the instantaneous star formation rate in dwarf galaxies at a particular time is a stochastic sampling of an underlying probability distribution of star formation rates. Of course, this view is only sensible as an approximation; nevertheless, there are benefits to thinking of star formation in this way, particularly as it pertains to generating analytic and semi-analytic models (Kelson et al. 2016).

Under this probabilistic interpretation, a galaxy's star formation rate represents a sampling of an underlying star formation rate probability distribution function. Our result suggest that the probability of galaxies being in the "central" state is 1.5 times higher as the galaxies in the "outer" state. We draw a distinction between these phase transitions and final quenching, when a galaxy becomes "red and dead." This final quenching phase is likely not a result of stochastic sampling of an underlying pdf, but rather the result of physical processes that bring the galaxy out of the "breathing" mode and into the "red and dead" mode. In particular, galaxies at these masses are predominantly quenched through environmental means (Kauffmann et al. 2003; Geha et al. 2012).

Physically, we can interpret the galaxy's duty cycle in terms of the times that galaxy spends in each phase in order to explore the physical scalings and energetics involved. As an example, we use the test case of a $10^9 M_\odot$ galaxy of radius 5 kpc. Assuming that the blowout moves with the speed v_{wind}, the total time it takes to reach the galaxy edge is $\frac{R}{v_{wind}}$. If the material takes the same amount of time to fall back onto the center as to reach the galactic outskirts[3], then the total time spent in the passive phase is twice this time. Using the duty cycle implied by Figure 14, we can conclude empirically that the time spent in the central phase during a single burst

[3] It's worth noting that, in the FIRE simulations, the recollapse is slower than the initial expulsion

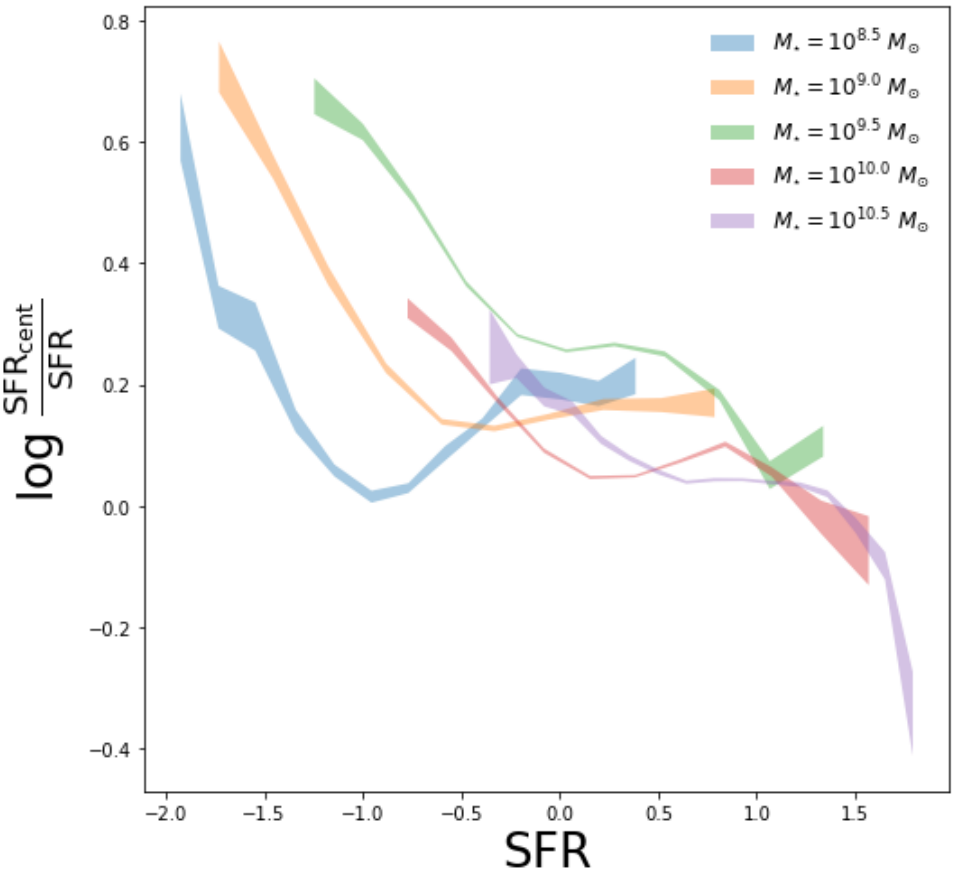

Figure 12. Ratio of $\frac{SFR_{cent}}{SFR}$ plotted against star formation rate for galaxies in the five mass bins. Galaxies in the lowest mass bins show no correlation or a slight positive correlation, while more massive galaxies show a negative correlation.

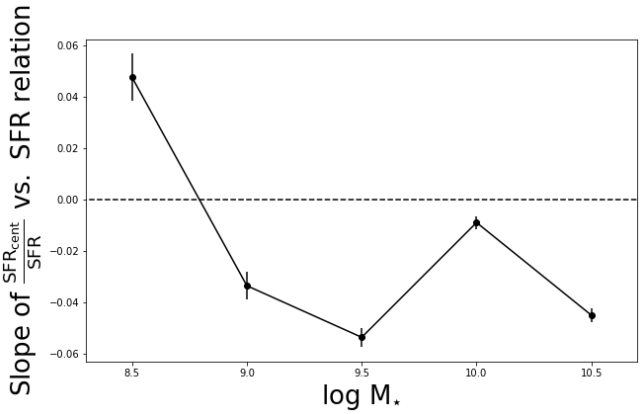

Figure 13. Slope of the $\frac{SFR_{cent}}{SFR}$ ratio vs. star formation rate relation plotted against stellar mass. The dwarf galaxy points are higher than the points corresponding to more massive galaxies.

is

$$t_{active} = .6 \times \frac{2 \times R}{v_{wind}} = 195.Myr \times \frac{R}{5kpc} \times \frac{30km/s}{v_{wind}},$$

consistent with the timescales put forward by El-Badry et al. (2016). Multiplying this value by the star formation rate of objects in the active phase gives us the total number of stars formed in one cycle:

$$\Delta M_\star = 3.51 \times 10^7 M_\odot \times \frac{SFR}{0.180 M_\odot/yr} \times \frac{t_{active}}{195 Myr}$$

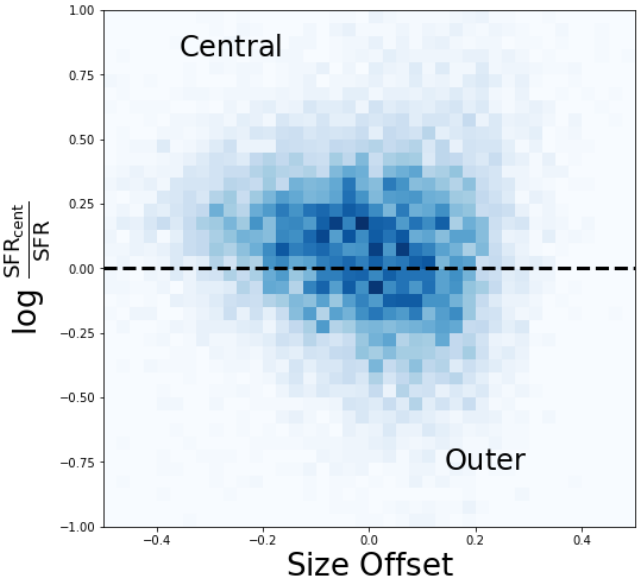

Figure 14. Black line divides the lowest mass sample into centrally-star forming galaxies and galaxies forming stars in their outer regions, Approximately 60% of the sample is in the central regime, while 40% is in the outer regime.

.

The IMF allows us to connect the amount of star formation in a burst to the strength of the supernova feedback produced by that burst. Under a Kroupa IMF

(Kroupa 2002), we expect one Type II supernova for every 100 solar masses in stars formed, meaning that a single burst in a dwarf galaxy produces some 3.5×10^5 Type II supernova. Given that the average energy output of a Type II supernova is 10^{51} erg, the total energy output during a single burst is 3×10^{56} erg. In order to produce $10^{8}.5 M_{\odot}$ of stellar mass, the galaxy must have gone through 10 cycles, thereby producing 3×10^{57} erg of supernova energy in the process during these episodes of centralized star formation. The energetic argument presented in the above paragraph is true independent of whether the stars are formed constantly or in bursts. However, as several authors have argued (Governato et al. 2012; Garrison-Kimmel et al. 2013), the "bursty" mode of star formation can produce a positive feedback cycle, where the the efficiency of subsequent bursts increases from the initial burst (see Pontzen & Governato 2012b; Governato et al. 2012).

4.3. *Comparisons to Simulations*

Hydrodynamical simulations whereby galaxy growth is regulated through burst-driven radial transport make a number of specific, testable predictions of galaxy observables. We divide our discussion of these predictions into two sections: predictions concerning galaxy dynamics, which we do not address but is addressed by Cicone et al. (2016), and predictions concerning galaxy structure, which is the primary concern of this work.

The burst-driven transport model of galaxy self-regulation requires that feedback not only couple to the gas in a galaxy, but also to the stellar component. As a result, the stars are kinematically heated, resulting in an increased line of sight velocity dispersion. El-Badry et al. (2017) makes this prediction explicit, demonstrating a correlation between σ_{LOS} and specific star formation rate for star particles in the final 40 snapshots of one simulated dwarf galaxy halo. Under the assumption that the evolution of this single halo is an ergodic process, this supplies a prediction for the population of dwarf galaxies at low redshift.

These predictions are borne out by the analysis of Cicone et al. (2016), which uses stacked SDSS spectra to examine the profiles of nebular emission lines and stellar absorption lines, constraining the dynamics of galactic gas and stars respectively. They find that, for dwarf galaxies, the width of stellar absorption lines increases with increasing specific star formation rate, consistent with the predictions of El-Badry et al. (2017). Furthermore, they find that this trend disappears above stellar masses of $10^{9.5} M_{\odot}$, consistent with the prediction that burst-driven transport only operates at dwarf mass scales.

On the other hand, Patel et al. (2018) claim they see no evidence for a breathing mode of star formation among isolated intermediate-mass galaxies in COSMOS. We do agree that the evidence for this breathing mode is not very convincing at the mass range $(10^9 - 10^{9.5} M_{\odot})$ they consider; however, the evidence is stronger at masses half a dex lower. In particular, we compare their Figure 3b with out Figures 13 and 12. While at high masses, we see no correlation between $\frac{SFR_{cent}}{SFR}$ and SFR, at lower masses, we see an increase in density among high star formation rate objects, consistent with a breathing-like process.

We can also compare the trends with size that we have explored in this work to predictions from hydrodynamical simulations. In Figure 15, we over plot sizes and star formation rates in the final 40 snapshots from the M10.6 (halo mass $\sim 10^{10.6}\ M_{\odot}$) galaxy in the FIRE simulation[4] (El-Badry et al. 2016), measured in such a way with as to mimic SDSS observations, alongside galaxies from our lowest-mass bin $(10^{8.5} - 10^{9.0} M_{\odot})$ in specific star formation rate/size space. Again, we emphasize that since the simulated galaxies evolve in this space, the points traced by the galaxy in the simulation make a prediction for galaxies sampled in the real Universe. We see agreement between the predictions made by the simulation and our observed relationship between specific star formation rate and size. There is significantly more scatter in the observed relation than the simulation results, which is a natural result of comparing an ensemble of galaxies with a single simulated object, but the overall agreement between simulations and data is striking. Taken together, these two observational confirmations of simulation predictions provide strong evidence that burst-driven radial transport is occurring in dwarf galaxies.

5. CONCLUSION

Our study primarily examines the relationship between the physical size of a galaxy and it's star formation properties. We show the following,

- The slopes of the star formation rate vs. size relations for galaxies binned by mass suggest that small-sized dwarf galaxies have more internal support, possibly from feedback, than small-sized, more massive galaxies.
- Comparisons of fiber-derived star formation rate to total star formation rate imply that star formation is centrally concentrated in small-sized galaxies in dwarf galaxies of mass $10^{8.5} - 10^{9}\ M_{\odot}$ and high star formation rate galaxies in dwarf galaxies of mass $10^{8.5} - 10^{9.5}\ M_{\odot}$
- Taken together, these results are consistent with a picture where dwarf galaxies experience cycles of star formation, where dense star formation in the central regions drives blowouts that self-regulate galaxy growth. However, we find, in agreement with Patel et al. (2018) that this effect does not impart a *strong* anti-correlation between star formation rate and size. However, we do see reasonable agreement with simulations that exhibit such blowouts.
- We find that the evidence from concentration is stronger than the evidence from size. Our ongoing work involves using slitless spectroscopy to localize star formation within dwarf galaxies to examine them for breathing-induced concentration effects.

REFERENCES

[4] These 40 snapshots are roughly evenly spaced between $z = 0$ and $z = 0.02$.

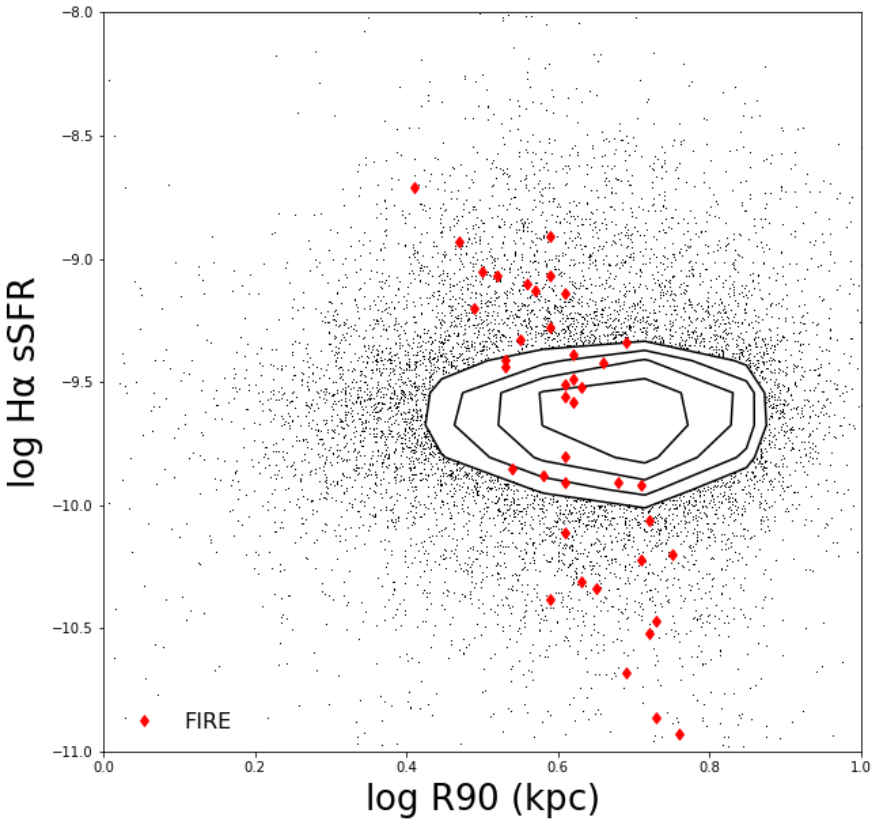

Figure 15. Star formation rate plotted against size for galaxies in our lowest mass bin. Overplotted are points from the last 40 snapshots of a dwarf galaxy in the FIRE simulation that is undergoing self-regulation via burst-driven radial transport. The data is in excellent agreement with the predictions from the simulations

Bakos, J., Trujillo, I., & Pohlen, M. 2008, ApJL, 683, L103
Baldwin, J. A., Phillips, M. M., & Terlevich, R. 1981, PASP, 93, 5
Balogh, M. L., Navarro, J. F., & Morris, S. L. 2000, ApJ, 540, 113
Bastian, N., Covey, K. R., & Meyer, M. R. 2010, ARA&A, 48, 339
Blanton, M. R., Schlegel, D. J., Strauss, M. A., et al. 2005, AJ, 129, 2562
Boselli, A., Boissier, S., Cortese, L., et al. 2009, ApJ, 706, 1527
Boylan-Kolchin, M., Bullock, J. S., & Kaplinghat, M. 2011, MNRAS, 415, L40
—. 2012, MNRAS, 422, 1203
Boylan-Kolchin, M., Springel, V., White, S. D. M., Jenkins, A., & Lemson, G. 2009, MNRAS, 398, 1150
Brinchmann, J., Charlot, S., White, S. D. M., et al. 2004, MNRAS, 351, 1151
Chan, T. K., Kereš, D., Oñorbe, J., et al. 2015, MNRAS, 454, 2981
Cicone, C., Maiolino, R., & Marconi, A. 2016, A&A, 588, A41
de Blok, W. J. G., Walter, F., Brinks, E., et al. 2008, AJ, 136, 2648
de Jong, R. S. 1996, A&A, 313, 377
Dekel, A., & Silk, J. 1986, ApJ, 303, 39
Di Cintio, A., Brook, C. B., Macciò, A. V., et al. 2014, MNRAS, 437, 415
El-Badry, K., Wetzel, A., Geha, M., et al. 2016, ApJ, 820, 131
El-Badry, K., Wetzel, A. R., Geha, M., et al. 2017, ApJ, 835, 193
Elbert, O. D., Bullock, J. S., Garrison-Kimmel, S., et al. 2015, MNRAS, 453, 29
Farouki, R., & Shapiro, S. L. 1981, ApJ, 243, 32
Garn, T., & Best, P. N. 2010, MNRAS, 409, 421
Garrison-Kimmel, S., Boylan-Kolchin, M., Bullock, J. S., & Kirby, E. N. 2014, MNRAS, 444, 222
Garrison-Kimmel, S., Rocha, M., Boylan-Kolchin, M., Bullock, J. S., & Lally, J. 2013, MNRAS, 433, 3539
Geha, M., Blanton, M. R., Yan, R., & Tinker, J. L. 2012, ApJ, 757, 85
González-Samaniego, A., Avila-Reese, V., & Colín, P. 2016, ApJ, 819, 101
Governato, F., Brook, C., Mayer, L., et al. 2010, Nature, 463, 203
Governato, F., Zolotov, A., Pontzen, A., et al. 2012, MNRAS, 422, 1231
Gunn, J. E., & Gott, III, J. R. 1972, ApJ, 176, 1
Guo, Y., Rafelski, M., Faber, S. M., et al. 2016, ApJ, 833, 37
Hidalgo, S. L., Aparicio, A., Martínez-Delgado, D., & Gallart, C. 2009, ApJ, 705, 704
Hidalgo, S. L., Monelli, M., Aparicio, A., et al. 2013, ApJ, 778, 103
Kauffmann, G., Heckman, T. M., White, S. D. M., et al. 2003, MNRAS, 341, 54
Kelson, D. D., Benson, A. J., & Abramson, L. E. 2016, ArXiv e-prints, arXiv:1610.06566
Kennicutt, Jr., R. C. 1998, ARA&A, 36, 189
Klypin, A. A., Trujillo-Gomez, S., & Primack, J. 2011, ApJ, 740, 102
Kroupa, P. 2002, Science, 295, 82
Larson, R. B. 1974, MNRAS, 169, 229
Larson, R. B., Tinsley, B. M., & Caldwell, C. N. 1980, ApJ, 237, 692
Lee, J. C., Gil de Paz, A., Tremonti, C., et al. 2009, ApJ, 706, 599
Lovell, M. R., Frenk, C. S., Eke, V. R., et al. 2014, MNRAS, 439, 300
Marchesini, D., D'Onghia, E., Chincarini, G., et al. 2002, ApJ, 575, 801

Maxwell, A. J., Wadsley, J., Couchman, H. M. P., & Mashchenko, S. 2012, ApJL, 755, L35
McGaugh, S. S., Rubin, V. C., & de Blok, W. J. G. 2001, AJ, 122, 2381
Moore, B. 1994, Nature, 370, 629
Moore, B., Katz, N., Lake, G., Dressler, A., & Oemler, A. 1996, Nature, 379, 613
Navarro, J. F., Eke, V. R., & Frenk, C. S. 1996, MNRAS, 283, L72
Navarro, J. F., Frenk, C. S., & White, S. D. M. 1997, ApJ, 490, 493
Patel, S. G., Kelson, D. D., Diao, N., Tonnesen, S., & Abramson, L. E. 2018, ArXiv e-prints, arXiv:1807.02118
Pontzen, A., & Governato, F. 2012a, MNRAS, 421, 3464
—. 2012b, MNRAS, 421, 3464
—. 2014, Nature, 506, 171
Schroyen, J., De Rijcke, S., Koleva, M., Cloet-Osselaer, A., & Vandenbroucke, B. 2013, MNRAS, 434, 888
Shivaei, I., Reddy, N. A., Shapley, A. E., et al. 2015, ApJ, 815, 98
Simon, J. D., Bolatto, A. D., Leroy, A., Blitz, L., & Gates, E. L. 2005, ApJ, 621, 757
Sparre, M., Hayward, C. C., Feldmann, R., et al. 2017, MNRAS, 466, 88
Springel, V., White, S. D. M., Jenkins, A., et al. 2005, Nature, 435, 629
Stinson, G. S., Dalcanton, J. J., Quinn, T., et al. 2009, MNRAS, 395, 1455
Sullivan, M., Treyer, M. A., Ellis, R. S., et al. 2000, MNRAS, 312, 442
Wambsganss, J., Bode, P., & Ostriker, J. P. 2004, ApJL, 606, L93
York, D. G., Adelman, J., Anderson, Jr., J. E., et al. 2000, AJ, 120, 1579